Correction notice

Extensive dynamic thinning on the margins of the Greenland and Antarctic ice sheets

Hamish D. Pritchard, Robert J. Arthern, David G. Vaughan & Laura A. Edwards

In the version of the Supplementary Information originally posted online, there were minor errors in Supplementary Tables 2 and 4, and in Supplementary Fig. 8. These have been corrected in the new version of the Supplementary Information; see Supplementary Information Table of Contents for details.

Methods

Interpolation

We used ICESat GLA12 Release 28 data[32] (at the highest calibration level 4), for all lasers in all available years from February 2003 up to November 2007. To quantify elevation change, we began by grouping ICESat height measurements into two-year epochs (2003-4, 2004-5, 2005-6 or 2006-7). We interpolated surfaces between all elevation measurements in an epoch that have two neighbours lying within 300 m distance, using triangular irregular networks (TINs). This ensures an interpolation distance never greater than 260 m, typically much shorter. For comparison, crossover analysis interpolates over ~172 m and uses four points rather than our three. Our scheme produces long, ribbon-like, linearly-interpolated surfaces between closely-spaced, near-parallel tracks representing surface height for each epoch. To account for the difference in timing of the measurements, we performed the same interpolation on acquisition date (Supplementary Figure 1 and 2).

Where these ribbon-like TINs were crossed by ground-track footprints from a later or earlier epoch, we extracted the interpolated elevation and acquisition date from the TIN at the new sample-point. This yields comparable elevation measurements: one interpolated, one measured precisely (crossover analysis compares pairs of interpolated heights), from which we calculated $\Delta h/\Delta t$ (Supplementary Figure 1). We repeated this for all possible date combinations forwards and backwards in time. The interval, Δt, ranges from 1 to 4.5 years, mean 746 days over Greenland, 728 days over Antarctica. Within a given epoch, this approach assumes linear elevation change both spatially

between adjacent points, and through time. It sacrifices temporal resolution to gain spatial coverage. A broadly similar approach has been developed independently and applied to several Greenland glaciers[33].

Uncertainty estimate

ICESat elevation precision and accuracy are slope-dependent and the dominant biases come from pointing errors, saturation errors and forward scattering. Pointing errors have been found to cause height bias across the range of ice sheet surface slopes of up to ±0.2 m over a period of days, causing height change errors of -0.03 to +0.11 m (mean ~0.03 m) between two orbit periods separated by one year, but such errors are now largely corrected in calibration[34,35,36]. Signal saturation causes heights to be biased low by up to 1.5 m in this data release and affects 38% of our data, but this is mitigated by applying a saturation correction[37]. Only 1% of data required a correction >0.4 m and the RMS of the correction is 0.13 m. A further low bias is introduced by forward-scattering of the signal through cloud, measured as, respectively, -0.16 m through thick cirrus[32] and in excess of -0.2 m[38], which can appear as prominent height anomalies that vary locally and temporally. Measurement precision over the ice sheets for preliminary ICESat data, not corrected for pointing errors, saturation or forward scattering, was found to vary with surface slope from 0.14 to 0.59 m[39]. Release 28 data for the laser periods 3A and 3B, when corrected for pointing errors, have a crossover standard deviation of 0.2 m, and this falls to below 0.1 m when the saturation correction is applied[36].

In some studies[39,40,41], waveforms suspected of cloud contamination are removed before processing. To maximize coverage in data-sparse coastal areas with potentially

high rates of change, we retained these data at this stage. We removed gross height

errors that exceeded a threshold relative to existing DEMs. To limit further the error

from forward scattering and any residual error from the other sources, we filtered the

$\Delta h/\Delta t$ results, rejecting those outside ± 0.75 times the inter-quartile range from the

median over a 25 km radius of each point (typically rejecting 30% of measurements).

This reduced the $\Delta h/\Delta t$ standard deviation from 0.24 to 0.10 ma^{-1} in West Antarctica.

We then took the spatial mean of the filtered points over a radius of 10 km (typically

several thousand points).

In summary, our $\Delta h/\Delta t$ measurements are derived from height measurements

largely corrected for pointing and saturation errors. We believe the residual uncertainty

(1-sigma) is <0.1 m[36]. We assume forward scattering error to be temporally

uncorrelated, affecting either the earlier or later data in a $\Delta h/\Delta t$ measurement, and so

becomes random in sign. We filter out $\Delta h/\Delta t$ measurements that are anomalous relative

to a large neighbourhood and assume a remaining forward-scattering uncertainty of 0.1

m (1-sigma). Our $\Delta h/\Delta t$ measurements come from combinations of typically 3 from 14

orbit periods assumed independent in error. From this budget, we estimate the combined

$\Delta h/\Delta t$ uncertainty in our spatially averaged measurements to be ± 0.07 ma^{-1} at the 1-

sigma level (this is similar to the uncertainty of 0.1 ma^{-1} reported for a comparable

along-track $\Delta h/\Delta t$ method[33]).

We validate our measurements against independent, coincident field GPS data

and by calculating the track-to-track $\Delta h/\Delta t$ RMS (Supplementary Table 1, locations in

Figure 1b)). Our comparison to GPS $\Delta h/\Delta t$ measurements from 2005 to 2007 is limited:

the mean ICESat Δt within this time window is only 376 days, compared to a minimum

threshold of 365 days and a mean of 734 for this study as a whole. One GPS site lies on

an orbit crossover but the other two are ~7km from the nearest ICESat data, which are also distributed rather than single-location measurements. Nonetheless, the discrepancy ranges from 0.06 to 0.21 ma^{-1}.

As a further test of the potential magnitude of uncertainty, we calculated the ground-track to ground-track RMS in our filtered and averaged dataset, along three de-trended profiles of ~300 km length that run approximately perpendicular to visible track-to-track variations in West Antarctica. Profile 1 is in a higher accumulation area (300-400 mm w.e. a^{-1}, profiles 2 and 3 are in relatively low-accumulation areas (<200 mm w.e. a^{-1})[3] (Figure 3 (profile 3 crossing the GH and E'E'' divide not shown)). The $\Delta h/\Delta t$ RMS for profile 1 was 0.08 ma^{-1}, for profile 2, 0.01 ma^{-1} and for profile 3, 0.02 ma^{-1}. These signals will contain some genuine temporal variability in surface elevation plus measurement errors associated with each track, but support our uncertainty estimate.

Volume and mass calculations

Our measurements incorporate elevation changes caused by trends in glacier flow rate (dynamics) and SMB on a multi-annual timescale, superimposed with seasonal accumulation, compaction and melt of the snowpack, and sporadic, short-lived snowfall and drifting events. We aim to study the longer-term ice sheet trends, in particular those driven by changing dynamics. Our technique to measure volume change suppresses short-term sub-annual signals by combining many measurements from multiple stages within a 2-year epoch, differencing them from a similar sample from, on average, 2 years later, and spatially averaging the results. The largest seasonal signal in

our study is Greenland summer melt. To estimate the magnitude of the residual summer melt signal in our results, we performed a Monte Carlo analysis based on the ICESat measurement-date probability distribution, our interpolation rules and an idealised, regular summer melt. We found the residual variability on $\Delta h/\Delta t$ estimates to be 12% of summer runoff (where melt occurred, the Greenland mean summer runoff for 1991 to 2000 was 0.51 m w.e.a^{-1} [42]).

From elevation change we can calculate volume change directly, but converting to mass is more complex, requiring knowledge of the density of material lost or gained. Only rarely is density known or can be reasonably inferred but it is highly significant: in combination, fluctuations in accumulation and trends in snow/firn density could have raised or lowered the Antarctic ice sheet surface by up to 0.20 ma^{-1} between 1980 and 2004[43]. Within the longer-term multi-annual trends, it remains difficult to distinguish between volume changes driven by glacier dynamics and by sustained surface mass-balance change. We take three approaches to making this distinction: 1) we compare our height change measurements to available SMB data and identify areas with changes greater than the variability in SMB; 2) we segregate our measurements into fast and slow-flowing classes on the drainage-basin scale using available flow-rate data and identify significant differences between these classes; 3) we use our high-resolution results to compare directly the rates of elevation change on fast-flowing ice to neighbouring slower areas on the local, sub-glacier scale, an important advantage of these high-resolution data. Where we detect dynamic volume change, we can convert this to a mass change using the density of ice (917 kg m^{-3}). Elsewhere, where we are unable to make this distinction, we refrain from making the conversion from volume to mass.
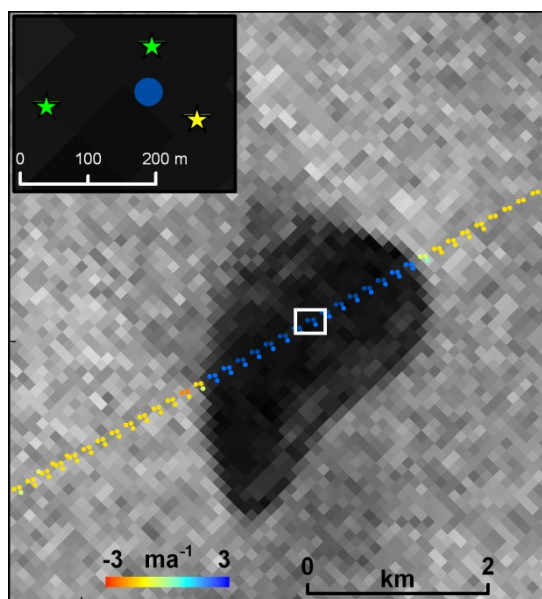
Supplementary Figures
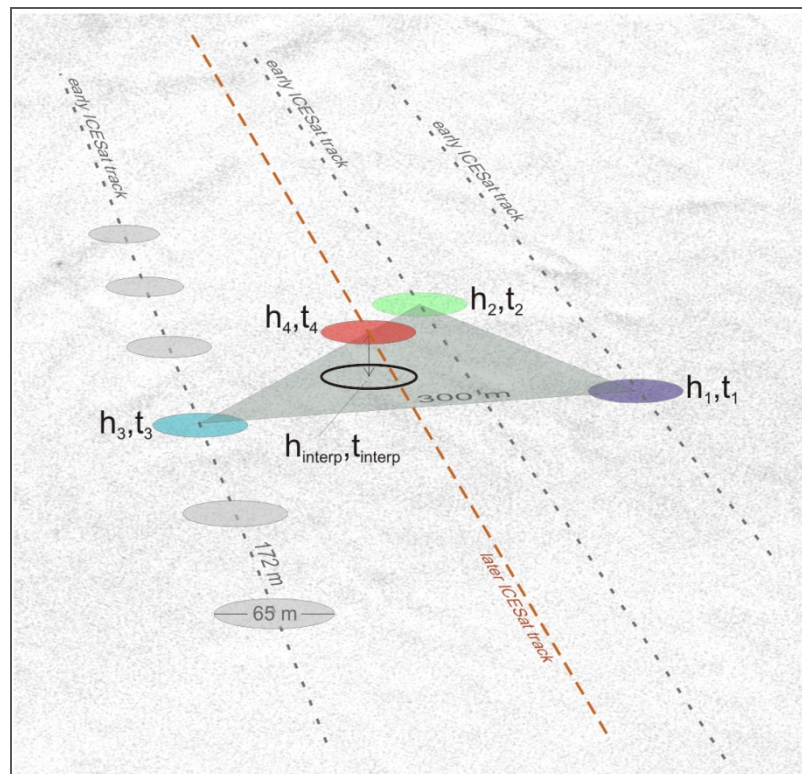
Supplementary Figure 1. ICESat interpolation scheme.

Our $\Delta h/\Delta t$ measurements are made between one measured and one interpolated point, each with the attribute of elevation and measurement date. In the example above, a triangular facet is fitted between three ICESat measurements that were acquired within the same two-year period (in this case from three separate passes). We do this for both height and measurement date. The maximum separation between points is 300 m (often shorter). A later ICESat pass overflies the facet and we compare the newly measured height and date to the linearly interpolated values to calculate $\Delta h/\Delta t$. Note that the triangular interpolation accounts for both across-track and along-track slope and linearly weights the height and date by proximity to a measured point. Our assumptions are that the slope covered by the facet is not curved and that the rate of height change between the three measurement dates that make up the facet is constant through time. Violation

of these assumptions is mitigated by spatial and temporal averaging of Δh/Δt

measurements. An example of this interpolation scheme is given below.

Supplementary Figure 2. Detail of melt pond filling and Δh/Δt measurement technique.

Figure 1 (main text) showed measurements of a melt pond filling in western Greenland. Here we show further detail of how these measurements were made, with a close-up of the melt pond (dark patch in background SAR image) and an individual Δh/Δt measurement (blue dot, inset). This individual Δh/Δt measurement was made using a single ICESat spot height of 1473.76 m from 15th March 2004, which was differenced from a triangular surface linearly interpolated from two points measured on 17th November 2005 (green stars, both 1478.72 m) and one measured on 20th November 2006 (yellow star, 1478.17 m). The interpolated height is 1478.47 m, the interpolated date is May 2nd, 2006, the Δh/Δt measurement is +2.21 ma^{-1}. This example shows the weaknesses and strengths of our technique: low temporal resolution but high spatial resolution, plus extensive coverage.
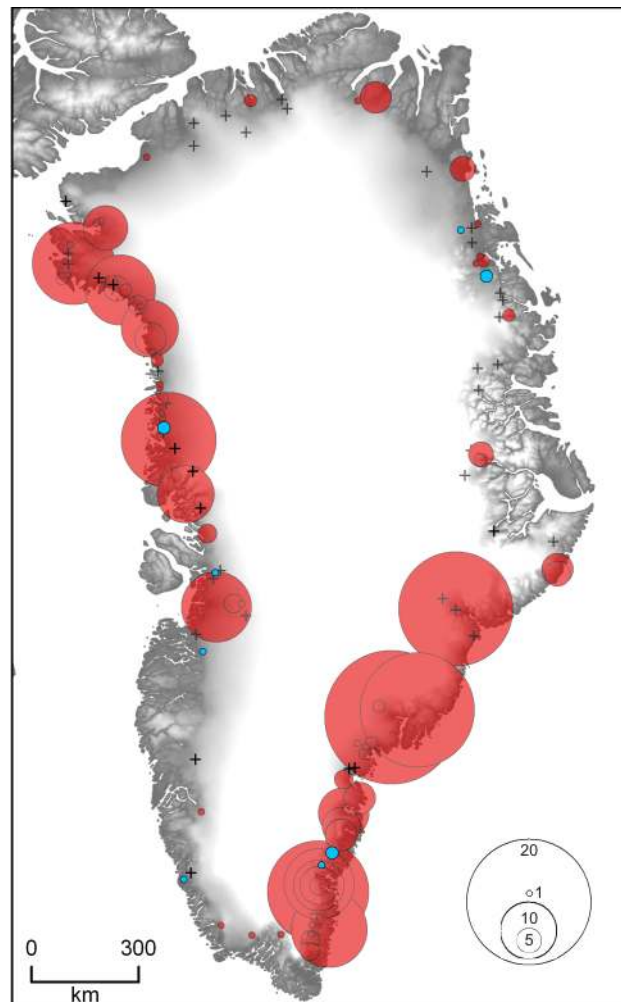
Supplementary Figure 3. Dynamically-driven elevation changes of Greenland outlet glaciers.

Rates of elevation change on Greenland outlet glaciers after removal of surface-mass-balance and density-change signals. Scale is metres per year, red shows thinning, blue thickening. Black crosses show surveyed glaciers where the dynamic rate of change is less than ± 1 ma^{-1}. The combined SMB and density-change signal was measured over slow-flowing ice at the same altitude and as close as possible to measurements made on outlet glaciers. Measurements on outlet glaciers are maxima for data averaged over 2 km, and where data coverage allows. Full details are given in Supplementary Table 5.
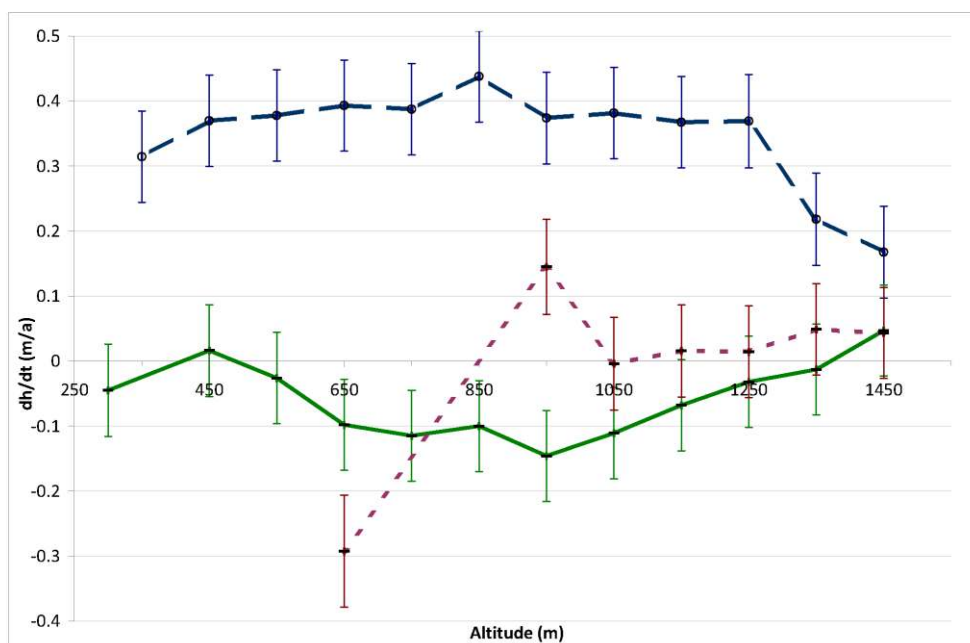
Supplementary Figure 4. Elevation change rates for the major land-terminating Greenland Ice Sheet margins.

Mean elevation change rates for the main slow-flowing, land-terminating margins, in 100 m altitude bins. Slow flow was identified from an interferometric velocity mosaic[44]. The green, solid line represents the northern margin (80 to 84°N), where the thinning maximum is at 900 m altitude (n=166568); the blue, dashed line represents the south-west margin (60 to 65°N), where thickening dominates throughout (n=110260); the red, dotted line represents the western margin (65 to 70°N), with a transition from strong thinning to slight thickening at high altitude (n=22274). Error bars are the standard errors of the mean combined with the estimated 0.07 ma^{-1} measurement error for a spatially averaged sample. The standard deviation of $\Delta h/\Delta t$ in each altitude bin ranges from 0.13 to 0.33 (80 to 84°N), 0.58 to 0.78 (60 to 65°N) and 0.31 to 0.78 (65 to 70°N). Changes over these slow-flowing areas are probably driven by SMB anomalies over the observed period.
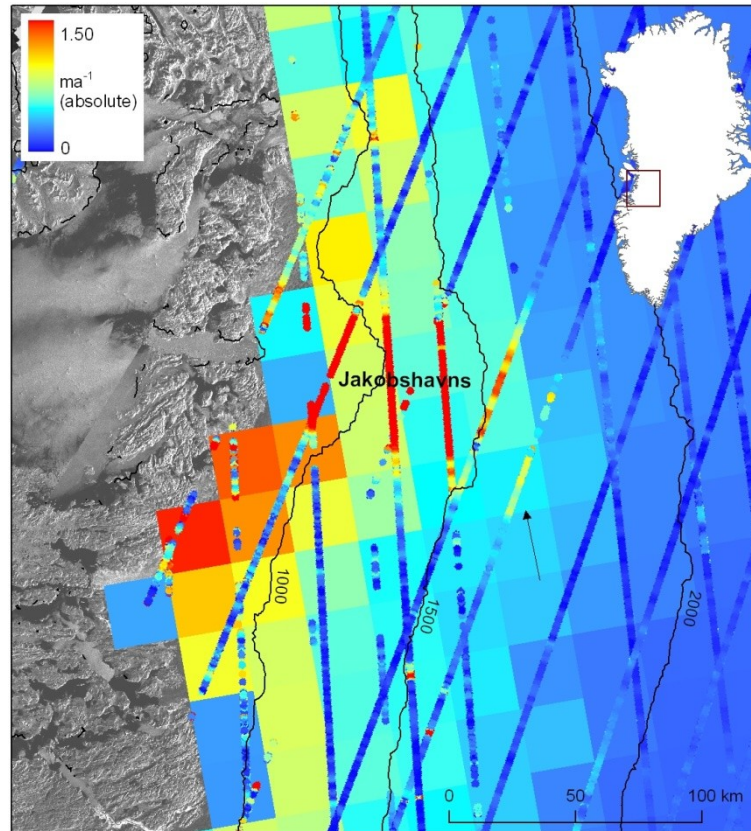
Supplementary Figure 5a

This figure shows the ICESat-derived absolute Δh/Δt values (tracks of data) for

Jakobshavn Isbræ drainage basin as absolute values, overlaid on a continuous grid of

the height variability due to interannual variation (the interannual standard deviation,

SD) in surface mass balance for the period 1991-2000[42]. We used a conservative density

of 400 kg m^{-3} to convert from metres water equivalent per year (m w.e. a^{-1}) to surface

height variability (m a^{-1}). Note that the ICESat Δh/Δt values over Jakobshavn are

actually negative and that they go far beyond the 1.5 ma^{-1} scale shown here. Surface

lowering is apparent in the ICESat data at rates beyond those expected from interannual

SMB variability at altitudes up to around 1600 m (arrowed). Furthermore, the ICESat

surface lowering in this area is greater than the lowering of areas at a similar altitude

adjacent to but outside of the main glacier drainage. At the arrowed location, mean

annual SMB was 0.04 m w.e. a^{-1} (SD=0.19) and mean accumulation was 0.27 m w.e. a^{-1}

(SD=0.09). Mean $\Delta h/\Delta t$ was -0.80 ma^{-1} (n=335, SD=0.29) over the faster flowing

glacier, and -0.07 ma^{-1} (n=909, SD=0.22) over the slow neighbouring areas. SMB

variability can explain the change over slow-flowing ice but not the much larger signal

on Jakobshavn, which we therefore ascribe to dynamic thinning. This location is around

120 km from the glacier front.
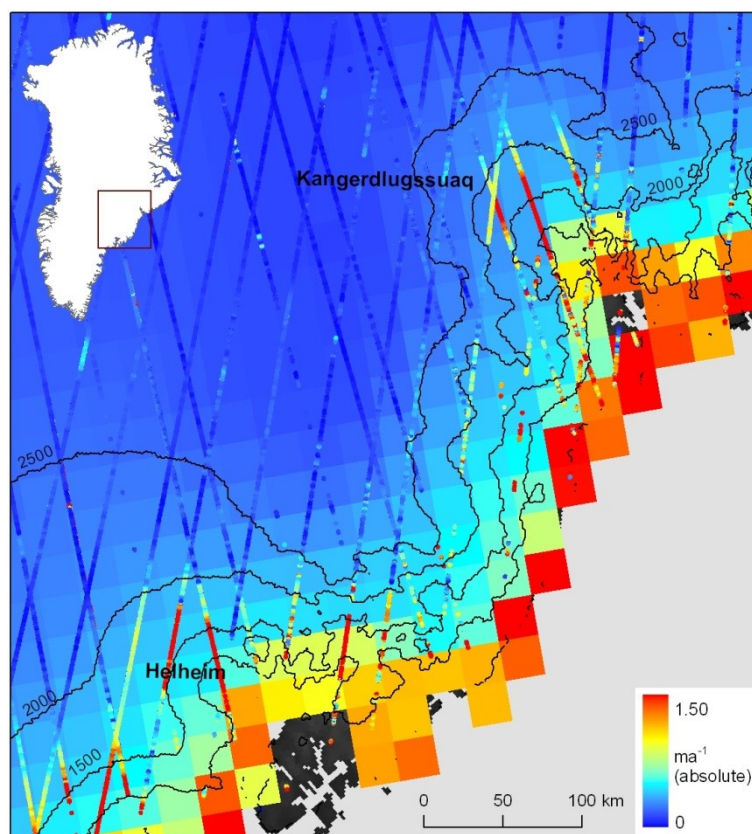
Supplementary Figure 5b

As for Supplementary Figure 5a, for Helheim and Kangerdlugssuaq glaciers. For

Helheim, thinning above the expected SMB-driven height variability (and at rates

greater than the neighbouring, slow-flowing ice) is evident up to the 2000 m contour

(note that a number of other dynamically-thinning glaciers lie to the south, hence slow-

flowing reference areas must be chosen with care in this figure). At this altitude, mean

SMB was around 0.74 ma^{-1} (SD=0.15) and mean $\Delta h/\Delta t$ was -0.79 ma^{-1} (n=1136,

SD=0.28) over the fast-flowing glacier, -0.41 ma^{-1} (n=1331, SD=0.24) over

neighbouring slow flow. The 2000 m contour is around 95 km from the front.

For Kangerdlugssuaq, surface lowering is also apparent at rates beyond those expected

from interannual SMB variability at an altitude above 2000 m. The mean SMB at this

altitude was 0.46 ma^{-1} with SD=0.13 (1991-2000) and for 2003 to 2008, Δh/Δt on the

fast-flowing glacier averaged -0.89 ma^{-1} (n=1366, SD=0.26) while on the slow-flowing

neighbouring areas, it was -0.34 ma^{-1} (n=1186, SD=0.20). Penetration of dynamic

thinning is detectable to around 100 km from the glacier front.
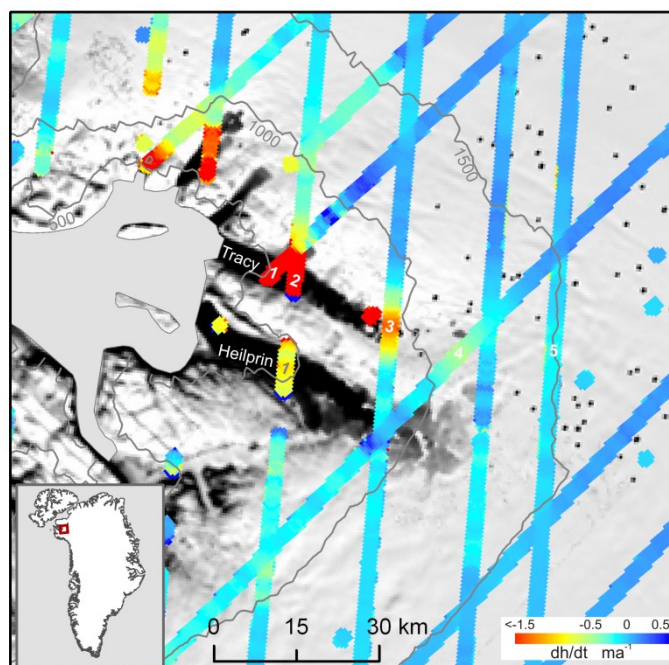
Supplementary Figure 6. Dynamic thinning detail, northwest Greenland.

Elevation change (colour) and flow rate for Tracy and Heilprin glaciers, northwest Greenland

(77.6 N). Black shows area of flow >100ma-1. Sites 1-5 are described in Supplementary Table

4. Contours are altitude (m).
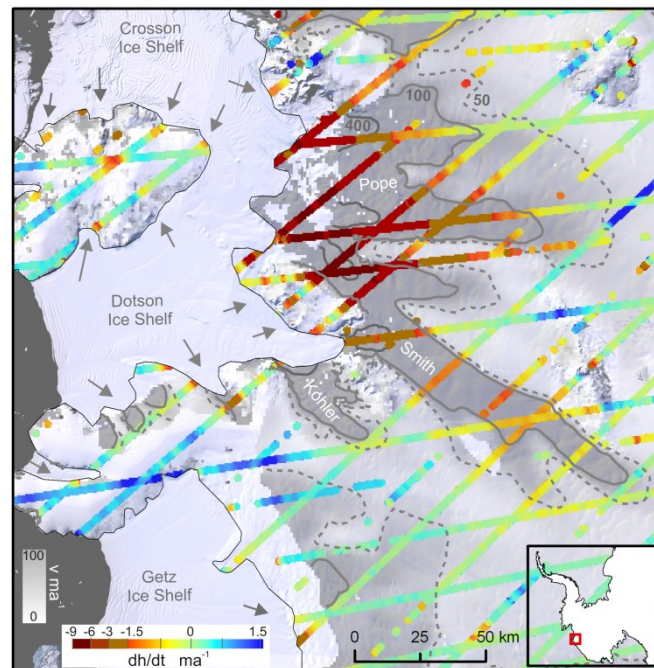
Supplementary Figure 7. Thinning of Smith, Kohler and Pope glaciers, Amundsen Sea Coast, West Antarctica. Upstream of the grounding line (black), these glaciers are thinning rapidly (colour bar) over areas of fast flow (grey shading and contours (interferometric velocity mosaic, partial coverage)), with the fastest thinning (9 ma^{-1}) coinciding with the fastest flow (~400 ma^{-1}). The lower reaches of multiple smaller, independent shelf-tributary glaciers (arrowed) are also thinning while adjacent, slow flowing areas change little or thicken. This spatial pattern is diagnostic of dynamic thinning driven by weakening of the floating ice shelf, which has been found to be thinning at up to 18±8 ma^{-1} [45]. In the case of Smith Glacier, dynamic thinning is detectable to 160 km upstream of the grounding line.
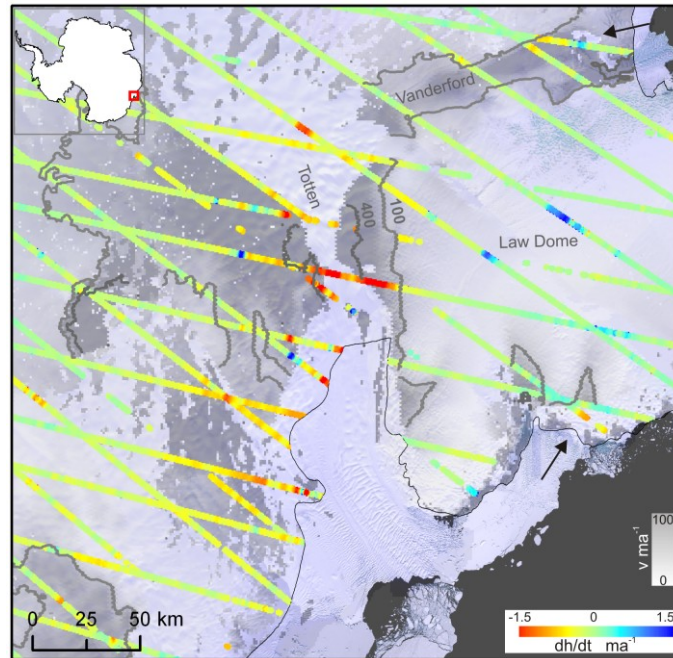
Supplementary Figure 8. Thinning of Totten Glacier, East Antarctica.

Totten Glacier, with the highest flux in East Antarctica, is thinning at up to 1.9 ma[-1] over areas of fast flow (grey shading and grey velocity contours lines (partial coverage)). This thinning rate is approximately three times greater than reported for the decade to 2004[45]. Neighbouring Vanderford Glacier and a small outlet of Law Dome (arrowed) also show a clear association between thinning and fast flow, indicating a common, ocean-driven cause of regional ice loss through dynamic thinning.
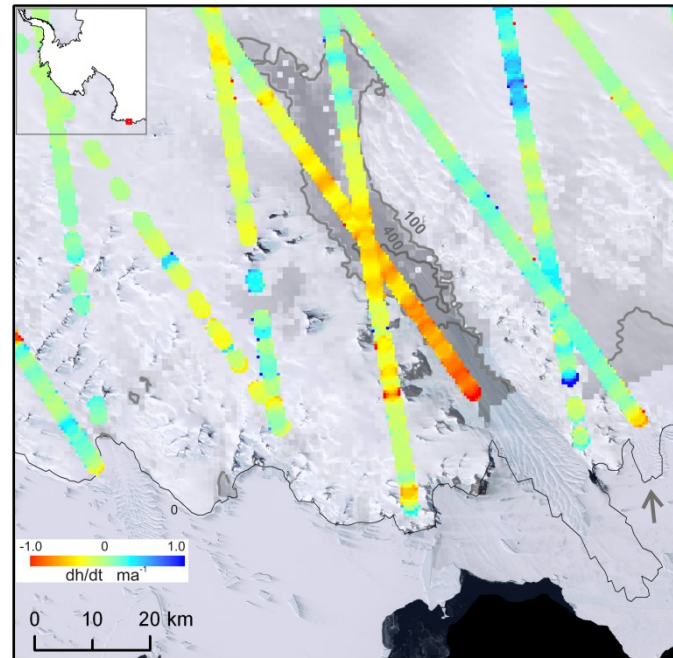
Supplementary Figure 9. Thinning of an East Antarctic outlet glacier, Oates Land coast. Thinning increases down-flow on the fast-flowing glacier trunk in contrast to neighbouring, slow-flowing areas. A nearby site (arrowed) independently shows similar behaviour. Velocity scale and velocity contours as for Supplementary Figure 8. Location is 69.3952°S, 157.3915°E.
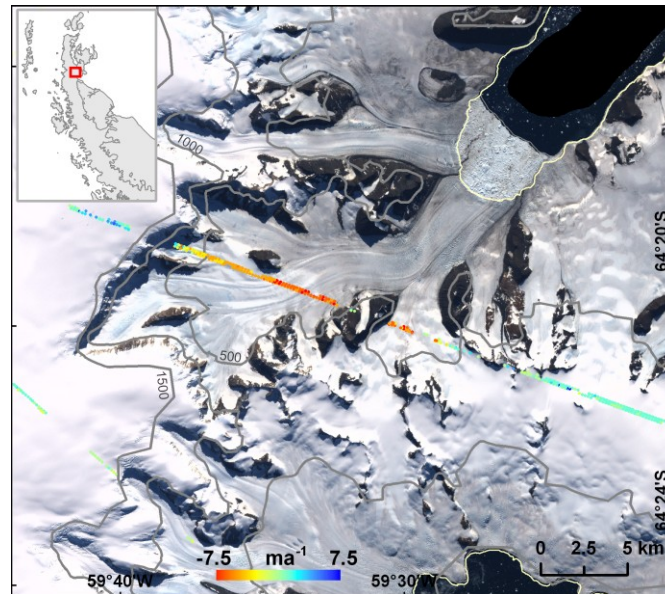
Supplementary Figure 10. Thinning of Sjögren Glacier, Antarctic Peninsula.

Following collapse of the Prince Gustav Ice Shelf in 1993, Sjögren Glacier is still thinning strongly right up to the glacier headwall (contours are altitude (m), white line shows current ice front). Full-resolution, non-averaged data.

Supplementary Tables

Supplementary Table 1. ICESat to GPS measurement comparison.

Location	GPS Δh/Δt (2005-2007) (ma[-1])	ICESat Δh/Δt (2005-2007)		
		Mean (ma[-1])	SD (ma[-1])	Sample size
Jurassic Nunatak (JN) (74º26S, 74º26W)	+0.005 ± 0.05	+0.13	0.18	286
Dyer Plateau (DP) (70º40S, 64º52W)	-0.015± 0.05	+0.04	0.19	218
Gomez Nunatak (GN) (73º59S, 70º36W)	-0.047± 0.44	+0.14	0.08	430

Comparison of a subset (2005-2007 only) of our ICESat results to GPS field measurements of height change rate on sites chosen as flat and distant from rock outcrops (locations JN, DP and GN in Figure 1b (inset)). Jurassic Nunatak GPS site lies on an ICESat crossover but Dyer lies at 7.5 km and Gomez at 6.5 km from the nearest Δh/Δt measurements, that are taken from within a 20 km radius of the GPS sites. Although the sample sizes are small, the time interval short (average of 376 days, only half the average period used throughout) and the GPS are point measurements while those from ICESat are distributed, the comparison shows reasonable agreement.

Supplementary Table 2. Elevation change rate by flow rate, compared to surface mass balance, Greenland Ice Sheet.

	Fast flow		Slow flow	
	Mean	SD	Mean	SD
Accum. (m w.e. a^{-1}) (1991-2000)	0.24	0.04	0.16	0.02
Runoff (m w.e. a^{-1}) (1991-2000)	0.34	0.10	0.32	0.08
SMB (m w.e. a^{-1}) (1991-2000)	-0.12	0.13	-0.18	0.10
Mean height (m)	930	473	1190	457
Area (km^2)	62500		291400	
SMB/runoff variability (ma^{-1})	0.18		0.12	
Detection threshold (ma^{-1})	**0.19**		**0.14**	
Δh/Δt (ma^{-1}) (2003-2007)	**-0.84**	1.97	**-0.12**	0.66
Samples	243041		1209642	

Here we compare elevation change rates (2003 to 2007) with available surface mass balance (SMB) statistics for Greenland (from 1991 to 2000)[42], for fast and slow-flowing areas (greater and less than 100 ma^{-1} respectively) for which flow data are available[44] (primarily along the coast). The accumulation, runoff and SMB standard deviations are interannual, not spatial. They cover a period preceding our Δh/Δt measurements and so we use them only to indicate the expected magnitude of interannual variability in these parameters for our study area. The 'SMB/runoff variability' value shows the expected variability in surface height for the slow and fast classes respectively that is due to the

combined effects of this expected interannual variation in surface mass balance and our sampling of the seasonal runoff signal, for the available data (for 1991-2000) and assuming an average snow density of 500 kg m^{-3} (see the Volume and Mass Calculation section of the Methods regarding our sampling of the runoff signal). The 'Detection threshold' value combines this with the 0.07 ma^{-1} measurement uncertainty. The fast and slow areas have similar altitudes and SMB characteristics but the fast-flowing area had thinning rates substantially greater than the detection threshold. In contrast, the average surface height change rate for the slow-flowing area is below the detection threshold. Furthermore, the difference in mean $\Delta h/\Delta t$ between fast and slow flow (0.72 ma^{-1}) is three times the expected RMS of surface height variability from the combined measurement uncertainty and SMB/runoff signals (0.24 ma^{-1}) (even under the conservative assumption that errors and SMB variations for fast and slow flow are not correlated). These observations strongly support the assertion that the fast-flowing areas along the Greenland ice sheet margins are thinning dynamically.

Supplementary Table 3

Glacier	Accel.[10] 2000-2005 (%)	Site	Altitude (m)	$\Delta h/\Delta t$ (ma^{-1})	$\Delta h/\Delta t$ SD	$\Delta h/\Delta t$ samples	SMB mean (m w.e. a^{-1})	SMB SD
Tracy	40	1	500	-7.29	0.36	61	-0.56	0.19
		2	600	-5.46	0.32	27	-0.56	0.19
		3	900	-1.26	0.17	178	-0.02	0.21
		4	1150	-0.46	0.09	646	-0.06	0.21
		5	1500	-0.17	0.09	419	0.18	0.08
Heilprin	18	1	450	-0.77	27	207	-0.48	0.15

Northwest Greenland glaciers Tracy and Heilprin accelerated 40% and 18% between 2000 and 2005[44] and also thinned, as shown above. SMB statistics are for 1991-2000[42]. On Tracy Glacier, thinning declines exponentially with altitude but exceeds the likely variability in surface mass balance up to at least 900 m altitude, for reasonable density values and accounting for a possible 20% decrease in SMB in the 2003-2007 period[46]. The spatial distribution of $\Delta h/\Delta t$ shown in Supplementary Figure 6, however, shows a thinning anomaly at site 4 (1150 m altitude), aligned with the fast-flowing trunk of Tracy Glacier, that we also attribute to the acceleration in flow. Locations of glaciers are given in Supplementary Table 5.

Supplementary Table 4. Antarctic sectors of significant thinning and thickening related to flow speed

Drainage sector	>100 ma^{-1}				<100 ma^{-1}				% basin area sampled
	Mean speed (ma^{-1})	Mean Δh/Δt (ma^{-1})	SMB height variab. (ma^{-1})	Detection threshold (ma^{-1})	Mean speed (ma^{-1})	Mean Δh/Δt (ma^{-1})	SMB height variab. (ma^{-1})	Detection threshold (ma^{-1})	
AA'	170	0.10	0.12	0.14	29	0.03	0.11	0.13	35
A'B	195	0.15	0.11	0.13	20	0.07	0.09	0.11	44
BC	238	-0.01	0.09	0.12	27	0.05	0.06	0.09	27
CC'	190	-0.08	0.19	0.20	30	0.01	0.13	0.15	45
C'D	190	-0.10	0.23	0.24	34	0.04	0.18	0.19	28
DD'	170	0.03	0.17	0.18	22	0.06	0.12	0.14	61
D'E	169	-0.10	0.11	0.13	13	-0.01	0.08	0.10	71
EE'	233	-0.03	0.10	0.12	18	0.01	0.06	0.09	14
E'E"	278	0.03	0.07	0.10	22	0.08	0.08	0.11	67
E"F	267	0.03	0.07	0.10	17	0.03	0.08	0.11	96
FF'	166	-0.10	0.15	0.17	21	0.03	0.13	0.15	73
F'G	216	-0.23	0.21	0.22	32	0.02	0.18	0.19	63
GH	333	-0.78	0.24	0.25	33	-0.04	0.22	0.23	78
JJ"	210	0.08	0.16	0.17	21	0.10	0.14	0.16	38
J"K	208	0.10	0.07	0.10	17	0.07	0.05	0.09	28
KA	162	0.13	0.14	0.16	18	0.08	0.12	0.14	77
PIG	397	-1.02	0.27	0.28	35	0	0.25	0.26	76

Detection of dynamic thinning (beyond the detection threshold calculated from the measurement uncertainty and the variability in height due to accumulation variation) in fast flowing areas (orange). Blue shows dynamic thickening.

Here we classify our $\Delta h/\Delta t$ measurements as from fast or slow flowing ice (defined as greater or less than 100 ma^{-1} [47]). We obtained glacier flow rate measurements from a synthetic aperture radar interferometry mosaic covering 75% of Antarctica (after[48,49,50,51,52]). For the fast and slow-flowing areas respectively, we compare mean elevation change rate with the expected surface height variability due to inter-annual variations in accumulation combined with the measurement uncertainty. Surface height can also vary due to changes in temperature that affect the firn compaction rate, but this effect is far less significant than variations in accumulation[43]. The expected accumulation variability is based on accumulation rate measured from passive microwave emissivity[53] with a mean annual relative variability of 30%[54], scaled to the mean 2-year measurement interval of our $\Delta h/\Delta t$ results. We use a snow density of 350 kgm^{-3} to calculate conservatively the resulting variability in surface height. The drainage sectors are shown in Figure 2. This table shows that the fast-flowing areas of drainage sectors F'G and GH (which includes Pine Island Glacier (PIG)) are thinning at a rate greater than the inter-annual accumulation variability, hence the thinning is dynamic in cause. In contrast, the slow-flowing parts of these sectors show no significant change. Sector C'D, which includes Totten Glacier, is thinning but at a rate that is not significant on the 2-year time scale. This, however, is partly the result of incomplete coverage in flow rate measurements over the lower glacier where thinning is greatest, and where the spatial pattern of change indicates that the cause is dynamic (Supplementary Figure 8). Similarly for sector HH', where we detect rapid thinning consistent with a dynamic cause, flow rate data is absent. The sector highlighted in blue is thickening at or above the detection level. Note though that for the Siple Coast sector E'E", where Kamb Ice

Stream is thickening while Whillans Ice Stream thins (Figure 4), these strong contrasting signals average to show no significant change on the drainage-sector scale.

Supplementary Table 5. Inventory of dynamic change in coastal Greenland.

This table shows the elevation change rate (ma^{-1}) due to dynamic thinning ($\Delta h/\Delta t$ D) (after removal of SMB and density change effects ($\Delta h/\Delta t$ SMB)) at the locations (Lat D, Long D) and altitudes specified, for outlet glaciers of the Greenland Ice Sheet. Some glaciers have multiple measured sites (hence glacier names are repeated). The combined SMB and density change signal was defined as the change measured over nearby slow-flowing ice at the same altitude as measurements on the outlet glaciers, on a case-by-case basis. The values from this study are the maximum rates of change identified along the available ICESat tracks for each glacier; unsampled areas of the glacier may exceed these.

	Glacier	Lat D	Long D	Δh/Δt D	Δh/Δt SMB	Altitude
North	Heilprin	77.520724	-65.3628	-0.54	-0.25	450
	Tracy	77.656714	-65.7343	-7.00	-0.30	500
	Unnamed	77.700128	-66.9397	-1.70	-0.70	220
	Unnamed	77.779448	-66.5552	-1.00	-0.60	380
	Unnamed	77.831164	-67.2071	-0.85	-0.05	1250
	Morris Jesup	77.87011	-71.2272	0.90	-0.50	110
	Humboldt	79.643744	-63.8909	-1.90	0.00	80
	Peterman	80.244222	-57.8319	-0.15	-0.15	800
	Peterman east tributary	80.796704	-58.6067	-0.45	-0.25	730
	Steensby	81.12837	-53.8706	-0.50	-0.05	870
	Ryder	81.570015	-50.1459	-2.20	-0.10	110
	Ryder	80.780742	-50.3988	-0.13	0.05	1450
	C.H. Ostenfeld (east)	81.407692	-43.9243	-0.30	-0.20	1000
	C.H. Ostenfeld (east)	81.643034	-44.7758	-0.75	-0.05	270
	Academy	81.383285	-32.1178	-1.44	-1.00	140
	Hagen	81.354977	-29.0912	-5.90	-0.40	500
	Nioghalvfjordsbrae	79.213734	-25.2426	-0.15	0.05	920
	Zachariae Istrom	78.943346	-20.7679	-4.40	0.10	90
	Storstrommen (upper)	77.564629	-23.8512	2.00	0.00	850
	Storstommen (stagnant)	77.171571	-23.1773	-0.40	-0.10	350
	Storstommen (stagnant)	76.788731	-22.9486	-1.50	-0.50	80
	Kofoed-Hansen	77.543744	-21.775	-1.90	-0.20	70
	Kofoed-Hansen	77.512022	-22.5762	-0.15	-0.05	460
East	Borgjokeln (land-term.)	76.664401	-23.6278	-1.20	-0.10	490
	L.Bistrup (stagnant)	76.653322	-22.8105	-2.70	0.10	130
	L.Bistrup (upper)	76.272877	-23.0847	2.15	0.00	630
	Ejner Mikkelsen (land term.) north	75.762458	-22.4041	-0.40	-0.40	340
	Ejner Mikkelsen (land term.) south	75.576086	-22.4495	-0.85	0.05	250
	Heinkel	75.223886	-23.3626	-0.40	0.05	1300
	Heinkel	75.170117	-22.4862	-2.40	-0.60	100
	Waltershausen	74.222344	-26.9163	-0.40	-0.10	1600
	Waltershausen	74.148795	-25.0824	-0.50	-0.40	840
	Unnamed	73.699289	-27.4269	-0.25	-0.55	860
	F. Graae	72.339888	-29.466	-0.20	-0.10	2000
	F. Graae	72.180378	-28.792	-4.20	-1.00	690
	Charcot	72.056774	-28.9993	-2.80	-1.50	390
	Daugaard-Jensen	71.796137	-30.4562	-0.30	-0.10	2000
	Vestfjord	70.296955	-29.4331	0.30	-0.70	780
	Dendritgletscher	69.620722	-25.6287	-0.85	-0.55	950
	Kangerdlugssuaq	68.681625	-33.289	-18.10	-0.40	840
	Kangerdlugssuaq	69.000546	-34.0106	-0.70	-0.20	1900
	Unnamed	68.954836	-26.0124	-5.40	-0.60	320
	Unnamed	68.857373	-26.0916	-4.80	-0.60	300
	Kong Christian IV	68.660077	-33.2881	-0.20	-0.70	980
	Polaric	67.957197	-32.4881	-0.40	-0.80	420
	Helheim	66.652115	-39.0385	-2.10	-0.30	1700
	Helheim	66.351288	-38.3681	-21.80	-1.20	340
	Midgardgletscher	66.446855	-36.7663	-18.90	-1.10	380

	Unnamed	65.817058	-40.5228	-1.30	-0.80	1610
	Unnamed	65.790208	-39.7043	-2.30	-0.80	1050
	Unnamed	65.708523	-40.051	-1.50	-0.80	1150
	Unnamed	65.556241	-40.1254	-2.85	0.25	880
	Unnamed	65.418814	-49.905	0.20	0.30	1000
	Unnamed	65.237247	-40.7758	0.30	-1.00	900
	Unnamed	65.22594	-41.0908	0.45	-2.75	840
	Unnamed	64.973907	-41.4434	-3.00	-0.60	1080
	Unnamed	64.508872	-40.6238	-5.30	-2.20	270
	Kangiatamunata sermia	64.176329	-49.3362	-1.10	-0.60	1000
	Gyldenlove Fjord	64.172483	-41.5696	-8.20	-2.30	350
	Bernstorff Isfjord north	63.868828	-41.7484	-6.10	0.10	400
	Bernstorff Isfjord south	63.658273	-41.7732	-5.75	-1.00	750
	Unnamed	63.667081	-41.7865	-5.70	-1.10	750
	Unnamed	63.248337	-42.2939	2.10	-2.00	390
	Unnamed	62.964752	-42.8761	1.20	-1.00	710
	Mogens Henesen Fjord north	62.520184	-43.0429	-11.50	0.10	70
	Mogens Henesen Fjord mid	62.487415	-43.053	-8.20	0.20	160
	Mogens Henesen Fjord south	62.343619	-43.0984	-16.20	-1.60	640
	Unnamed	62.488349	-43.0348	-6.30	-0.10	670
	Unnamed	62.488349	-43.0348	-3.50	-0.90	1060
	Unnamed	61.760313	-43.3468	-1.80	-0.80	1240
	Husfjeldet	61.677626	-43.2133	-2.00	-0.80	1250
	Unnamed	61.564045	-43.4225	-1.85	-0.80	1120
	Unnamed	61.443494	-42.6146	-12.30	-1.50	200
	Qorqup Sermia	61.344841	-44.991	-1.80	-0.40	900
	Unnamed	61.326389	-43.5142	-1.10	-1.30	890
	Unnamed	61.215193	-43.5551	-3.20	-1.00	1070
	Unnamed	60.944041	-43.6047	-3.80	-0.30	290
West	Eqalorutsit kitdlit sermiat	61.325203	-46.4221	-1.70	1.10	1100
	Unnamed	61.518984	-47.9658	-1.60	0.40	660
	Frederikshab Isblink	62.548439	-49.9907	1.70	0.40	480
	Frederikshab Isblink	62.71831	-49.6318	0.15	0.70	900
	Kangiatamunata sermia	64.176329	-49.3362	-1.10	-0.60	1000
	Unnamed	65.418814	-49.905	0.20	0.30	1000
	Unnamed	68.006468	-50.0219	1.10	-1.00	580
	Nordenskiold	68.40605	-50.5596	-0.40	-1.00	550
	Jakobshavns Isbrae	68.935389	-47.3423	-0.50	-0.10	1650
	Jakobshavns Isbrae	69.102998	-49.3684	-11.90	-1.20	490
	Jakobshavns Isbrae	69.213645	-48.2395	-3.50	0.00	1350
	Jakobshavns Isbrae	69.216017	-47.6838	-1.80	0.40	1530
	Eqip Sermia	69.787337	-49.7242	-0.60	-0.40	890
	Kangilerngata sermia	69.928979	-49.6351	1.60	-0.50	760
	Sermeq Kujatdleq	69.991589	-49.279	-0.80	-0.30	1180
	Kangigdleq	70.762119	-50.5415	-0.40	-0.80	500
	Sermeq silardleq	70.858802	-50.449	-3.80	-0.80	540
	Kangerdlugssuq sermerssua	71.467175	-51.1457	0.80	-1.80	290
	Umiamako Isbrae	71.757699	-52.428	-9.20	-1.10	370
	Rink Isbrae	71.778524	-50.5857	-0.30	-0.70	1070
	Unnamed	72.337723	-52.0827	0.15	-0.45	1300

Uperrnavik Isstrom south	72.826121	-53.7868	0.95	-1.80	675
Uperrnavik Isstrom	73.006481	-54.4284	-15.00	-2.00	130
Alangorssup sermia	73.169811	-54.9811	0.00	-1.90	260
Nunatakavsaup sermia	73.276904	-55.0161	2.90	-1.50	310
Kakivfait sermiat	73.500499	-55.2834	-1.15	-0.85	200
Qeqertarssup sermia	73.619459	-55.418	-1.50	-1.00	230
Ussing Braeer south	73.877429	-55.186	0.00	-0.55	620
Ussing Braeer	73.973351	-55.6354	-2.50	-0.70	410
Cornell Glet.	74.211831	-55.9947	-1.00	-0.80	230
Unnamed	74.305533	-56.0564	-1.60	-0.80	150
Unnamed	74.616444	-56.436	0.00	0.00	20
Hayes south	74.877584	-56.7312	-2.90	-1.80	160
Hayes central	74.998358	-56.8363	-0.30	-0.90	400
Hayes north	75.050608	-57.4208	-1.00	-1.30	200
Steenstrup south	75.13625	-57.5508	-0.60	-0.90	240
Steenstrup north	75.359756	-57.818	-5.10	-1.40	400
Unnamed	75.593573	-58.0988	-9.60	-1.70	130
Nansen Glet.	75.827135	-58.837	-0.10	-0.70	340
Kong Oscar Glet.	76.068507	-59.5144	-1.50	-0.50	410
Unnamed	76.095936	-59.8153	-3.20	-0.20	380
Unnamed	76.098289	-68.0795	-2.30	-0.50	370
Peary Glet.	76.158057	-60.5383	-1.80	-0.50	300
Unnamed	76.223642	-67.6746	-1.90	-0.70	200
Docker Smith Glet. south	76.325297	-61.975	-11.20	-2.30	140
Docker Smith Glet. north	76.359986	-61.4865	-2.10	-0.20	580
Unnamed	76.338028	-62.4129	-4.10	-0.50	250
Gade Glet.	76.398436	-62.8709	0.20	-0.50	270
Unnamed	76.405969	-63.6773	-0.60	-0.60	370
Unnamed	76.438615	-63.0761	-2.80	-1.20	150
Unnamed	76.440838	-64.5278	0.30	-0.30	510
Store Landglet. (land term.)	76.492156	-68.046	0.00	-0.40	500
Harald Moltke Br.	76.551115	-67.6046	-13.10	-0.50	200

Supplementary Table 6. Comparison of Greenland outlet glacier Δh/Δt rates to other studies[33,55,56]

This table compares Δh/Δt values for glaciers studied by Thomas et al. (2009)[55] and, where noted, Joughin et al. (2008)[56] and Howat et al. (2008)[33]. The comparison is approximate as surveys may differ in time and measurement locations in other studies are not precisely defined. These other studies do not distinguish the dynamic component of their height-change signal (ours are presented as 'Δh/Δt D'). Where samples come from a similar part of the glacier at a similar time, the values are broadly similar. A notable exception is Hagen Bræ, which appears to go from quiescence to surging between the studies. The values from this study are the maximum rates of change identified along the available ICESat tracks for each glacier.

Glacier	Thomas et al. Δh/Δt (ma⁻¹)	Comments	This study Δh/Δt (ma⁻¹)	This study Δh/Δt D (ma⁻¹)	Comments
Eqalorutsit kitdlit sermiat	~ -1	2001-2006 ~ 5km inland	-0.6	-1.7	Alt. 1100 m ~20 km inland
Kangiatamunata sermia	Up to -8	1998-2001 Seaward 3 km.	-1.7	-1.1	Alt. 1000 m ~28 km inland
Jakobshavn upper	Over -4	2005-2007 70 km inland	-3.5	-3.5	Alt. 1350 m ~80 km inland

Jakobshavn lower	~ -14 (over -10*)	2005-2007 ~30 km inland (*2005-2006, Joughin et al.[56])	-13.1	-11.9	Alt. 490 m ~30 km inland
Kangerdlugssup	Few tens of cm	2005-2006 Near coastal	-1.0	+0.8	Alt. 290 m ~13 km inland
Rink	Over -0.8	1998-2006 Within 40 km of coast.	-1.0	-0.3	Alt. 1070 m ~42 km inland
Upernavik	-1 to -2	1999-2002 Seaward 20 km	-3.8	-1.8	Alt. 500 m Seaward 20 km
Steenstrup	Up to -4	1999-2005 Near coastal	-6.5	-5.1	Steenstrup north. Alt. 400 m
Kong Oscar	Up to -1.5	1999-2005 Seaward 10 km	-2.0	-1.5	Alt. 410 m ~16 km inland
Humboldt	-1.1	1999-2007 Seaward 10 km	-1.9	-1.9	Alt. 80 m 13 km inland
Petermann	Slight thinning	2002-2007 Above grounding line	-0.3	-0.15	Alt. 800 m ~120 km inland
Steensby	-0.7	1999-2007 40 km inland	-0.55	-0.50	Alt. 870 m ~65 km

		Alt. ~650 m			inland
Ryder	~ -1	1999-2007 ~30 km inland	-2.3	-2.2	Alt. 110 m ~30 km inland
Hagan Bræ	0	1994-1999 30-60 km inland. Possible quiescent surge-type.	-6.3	-5.9	Alt. 500 m Approx. 50 km inland. Possible surge in progress.
Nioghalvfjordsbræ	-0.3	1999-2007 Seaward 150 km	-0.1	-0.15	Alt. 920 m ~120 km inland
Zachariae	Over -2	1999-2007 Near coastal.	-4.3	-4.4	Alt. 90 m Near margin
Storstrommen lower	Up to -2	1999-2007 Seaward 40 km	-2.0	-1.5	Alt. 80 m Near margin
Storstrommen upper	Up to +3	1999-2007 Inland of 40 km from front	+2.0	+2.0	Alt. 850 m ~100 km inland
L.Bistrup lower	Over -2	1999-2007 Seaward 40 km	-2.6	-2.7	Alt. 130 m ~17 km inland
L.Bistrup upper	Up to +2.5	1999-2007 Inland of 40 km from front	+2.15	+2.15	Alt. 630 m ~50 km inland

Vestfjord	Over -1	After 2001 Seaward 20 km	-0.4	+0.3	Alt. 980 m ~30 km inland
Kong Christian IV	-0.5	1998-2006 Inland of 20 km from front	-0.9	-0.2	Alt. 980 m ~40 km inland
Kangerdlugssuaq	-20 (~ -20)*	2005-2007 25 km inland. northern tributary. *(2002-2005, 25 km inland, location unspecified, Howat et al.[33])	-17.7	-18.1	Alt. 840 m ~25 km inland southern tributary
Helheim	~ -25 (~ -35)*	2003-2005 ~13 km inland *(2002-2005, ~13 km inland, Howat et al.[33])	-23.0	-21.8	Alt. 340 m ~13 km inland
Bernstorf	(~ -8)*	*(2002-2005, 750 m altitude, location unspecified, Howat et al.[33])	-6.75	-5.75	Alt. 750 m. (Bernstorf South)

32　　Zwally, H. J., R. Schutz, C. Bentley, J. Bufton, T. Herring, J. Minster, J. Spinhirne, and R. Thomas. GLAS/ICESat L2 Antarctic and Greenland Ice Sheet Altimetry Data V028. *Boulder, CO: National Snow and Ice Data Center. Digital media.* (2007).

33　　Howat, I. M., Smith, B. E., Joughin, I. & Scambos, T. A. Rates of southeast Greenland ice volume loss from combined ICESat and ASTER observations. *Geophys. Res. Lett.* **35** (2008).

34　　Luthcke, S. B., D.D. Rowlands, T.A. Williams, M. Sirota. Calibration and reduction of ICESat geoloaction errors and the impact on ice sheet elevation change detection. *Geophys. Res. Lett.* **32** (2005).

35　　Fricker, H. A., A. Borsa, B. Minster, C. Carabajal, K. Quinn, and B. Bills. Assessment of ICESat performance at the salar de Uyuni, Bolivia. *Geophys. Res. Lett.* **32**, L21S06, doi:doi:10.1029/2005GL023423. (2005).

36　　http://nsidc.org/data/icesat/detailed_disclaimer.html#SatCorrNote.

37　　Csatho, B., Y. Ahn, T. Yoon, C.J. van der Veen, S. Vogel, G. Hamilton, D. Morse, B. Smith, and V. B. Spikes. ICESat Measurements reveal Complex Pattern of Elevation Changes on Siple Coast Ice Streams, Antarctica. *Geophysical Research Letters* **32** (2005).

38　　Brenner, A. C. D., J.P. and Zwally, J.H. Precision and Accuracy of Satellite Radar and Laser Altimeter Data Over the Continental Ice Sheets. *IEEE Trans. Geosci. Remote Sensing* **45** (2007).

39　　Zwally, H. J., Yi, D. H., Kwok, R. & Zhao, Y. H. ICESat measurements of sea ice freeboard and estimates of sea ice thickness in the Weddell Sea. *J. Geophys. Res.-Oceans* **113**, 17, doi:C02s1510.1029/2007jc004284 (2008).

40　　Smith, B. E., C.R. Bentley, and C.F. Raymond. Recent elevation changes on the ice streams and ridges of the Ross Embayment from ICESat crossovers. *Geophys. Res. Lett.* **32**, art. no.-L21S09, doi:10.1029/2005GL024365 (2005).

41　　Kwok, R., Cunningham, G. F., Zwally, H. J. & Yi, D. Ice, Cloud, and land Elevation Satellite (ICESat) over Arctic sea ice: Retrieval of freeboard. *J. Geophys. Res.-Oceans* **112**, 19, doi:C12013 10.1029/2006jc003978 (2007).

42　　Box, J. E., Bromwich, D. H. & Bai, L.-S. Greenland ice sheet surface mass balance 1991-2000: Application of Polar MM5 mesoscale model and in situ data. *J. Geophys. Res.* **109** (2004).

43　　Helsen, M. M. *et al.*　　1153894 (2008).

44　　Rignot, E. & Kanagaratnam, P. Changes in the velocity structure of the Greenland ice sheet. *Science* **311**, 986-990 (2006).

45　　Rignot, E. & Jacobs, S. S. Rapid bottom melting widespread near Antarctic Ice Sheet Grounding lines. *Science* **296**, 2020-2023 (2002).

46　　Rignot, E., Box, J. E., Burgess, E. & Hanna, E. Mass balance of the Greenland ice sheet from 1958 to 2007. *Geophys. Res. Lett.* **35** (2008).

47　　Meehl, G. A., T.F. Stocker, W.D. Collins, P. Friedlingstein, A.T. Gaye, J.M. Gregory, A. Kitoh, R. Knutti, J.M. Murphy, A. Noda, S.C.B. Raper, & I.G. Watterson, A. J. W. a. Z.-C. Z. Global Climate Projections. In: Climate Change 2007: The Physical Science Basis. Contribution of Working Group I to the Fourth Assessment Report of the Intergovernmental Panel on Climate Change. [Solomon, S.,D. Qin, M. Manning, Z. Chen, M. Marquis, K.B. Averyt, M. Tignor and H.L. Miller (eds.)]. Cambridge University Press, Cambridge, United Kingdom and New York, NY, USA. (2007).

48   Joughin, I. & Tulaczyk, S. Positive mass balance of the Ross Ice Streams, West Antarctica. *Science* **295**, 476-480 (2002).

49   Joughin, I. & Padman, L. Melting and freezing beneath Filchner-Ronne Ice Shelf, Antarctica. *Geophys. Res. Let.* **30**, art. no. 1477 (2003).

50   Kwok, R. & Fahnestock, M. A. Ice sheet motion and topography from radar interferometry. *IEEE Trans. Geosci. Remote Sensing* **34**, 189-200 (1996).

51   Kwok, R., Siegert, M. J. & Carsey, F. D. Ice motion over Lake Vostok, Antarctica: constraints on inferences regarding the accreted ice. *J. Glaciol.* **46**, 689-694 (2000).

52   Jezek, K. RADARSAT-1 Antarctic Mapping Project: change-detection and surface velocity campaign. *Ann. Glaciol.* **34**, 263-268 (2002).

53   Arthern, R. J., Winebrenner, D. P. & Vaughan, D. G. Antarctic snow accumulation mapped using polarization of 4.3-cm wavelength microwave emission. *J. Geophys. Res.* **111** (2006).

54   Genthon, C. Space-time Antarctic surface mass-balance variability from climate models. *Ann. Glaciol.* **39**, 5 (2004).

55   Thomas, R., Frederick, E., Krabill, W., Manizade, S. and Martin, C. Recent changes on Greenland outlet glaciers. *J. Glaciol.* **55**, 16 (2009).

56   Joughin, I. *et al.* Continued evolution of Jakobshavn Isbrae following its rapid speedup. *J. Geophys. Res.* **113**, art. no.-F04006 (2008).